Electromagnetic and Thermal Analysis of Gas Insulated Substation (GIS)

A Project Proposal

Submitted in partial fulfillment of the

requirement for the award of degree

of

Master of Technology

by

Kulkarni Tushar Vilas

(Enrollment No.-14529008)

Under Supervision of:

Dr. Ganesh B. Kumbhar

DEPARTMENT OF ELECTRICAL ENGINEERING

INDIAN INSTITUTE OF TECHNOLOGY ROORKEE

November, 2015

Abstract

GIS is preferred to AIS now a days because it has many advantages over it viz. small space requirement, better insulation strength etc. Main components of GIS include electrical bus bars, circuit breakers, current transformers, voltage transformers, etc. The dielectric medium used in GIS is SF_6 which has many advantages over air viz. better insulation strength, chemical stability, non-inflammability, high lifetime etc.

The current carrying capacity i.e. Ampacity of any conductor is highly influenced by it's maximum operating temperature. Hence, from design point of view, it is important to know what temperatures a particular set of conductors of same dimensions would achieve while supplied with the same amount of electrical current. In this work, the same idea was implemented for single phase and three phase bus bars. A set of four metals viz. Aluminium 6063, Stainless steel, Mild steel, Aluminium AlMgSi were studied as potential choices for making conductors and enclosures of busbar. A particular value of AC steady steate current was allowed to flow through the conductors. The losses occuring in main conductors and in enclosures (due to induced eddy currents) were calculated using Maxwell Ansoft software. These loss values were used as inputs for thermal analysis and the subsequent temperature distribution across the cross section of bus bar was obained using Finite Element Method. The best metal of the four was then chosen based on temperature analysis.

Secondly, many contaminating particles are generated in GIS due to arcing. Surface of spacers or any other components are also non-uniform. Such non-uniformities or contamination due to particles present in SF_6 may lead to increased electric field and ultimately insulation failure. The effects of such non-linearity are studied by considering hemi spherical protrusions and depressions on the spacer surface. The effects of particle presence near the spacer surface are also studied. In both of the cases, the radius and the position of the defects along the spacer surface are varied and subsequent changes in the electric field intensity magnitude around the spacer surface are observed using Finite Element Method (FEM).

Contents

List of Tables

List of Figures

Chapter 1

Introduction

1.1 GIS vs AIS

Traditionally substations have been built in open premises where air is used as dielectric medium i.e.Air Insulated Substation (AIS). But AIS has following major issues

1. Environmental : Outdoor switchgear is directly exposed to effects of environmental conditions. Hence, they have to be designed considering both electrical and environmental specifications.

2. Space Requirement : Mandatory clearances have to be provided between phase conductors and also between phase to ground. So, the size of the installation increases as the voltage level goes up.

3. Geographical and social : Large area is required for setup of AIS. So, land acquisition, settlement of PAP's (project affected people) pose problems. In addition, the area needs to be levelled afterwards.

Figure 1.1.1: GIS vs AIS [1]

Comparatively, GIS has following advantages

1. Environmental : The components are surrounded by SF_6 gas used as dielectric. So, the environmental affects on the components are minimal.

2. Space requirement : SF_6 has better dielectric strength than air. So, the clearances required between phase conductors and between phase to ground are lower. Hence, the space required for GIS is only 10% of as that required by AIS of same rating.The relative size of GIS vs AIS is as shown in figure 1.1.1 [8].

3. Installation : As the space requirement for GIS is small, it can be setup near load centre e.g. in city. So, the T & D losses can be minimized.

1.2 GIS components

A typical Gas insulated Substation (GIS) consists of electrical bus bars, circuit breakers, current transformers, voltage transformer as shown in figure 1.2.1.

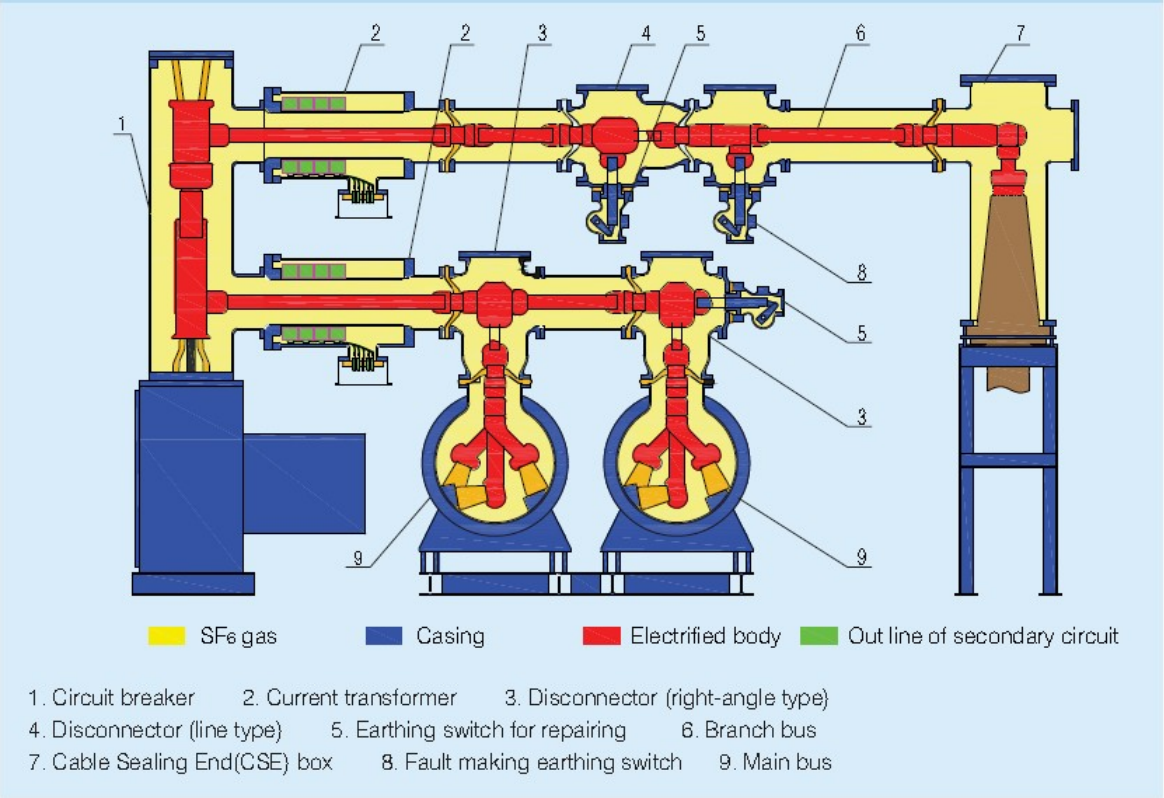

Figure 1.2.1: GIS components [1]

1.3 Literature Review

Temperature rise of the conductor is an important aspect while selecting any particular material for making conducting parts. It should be within tolerance limits according to IEC 60517 C 23 i.e. below 65^{o}C for conductos and inaccessible parts and below 30^{o}C for enclosures and accessible parts [2]. It was found that this temperature value can be found out by first calculating electrical loss value by

magnetic analysis and then using this loss value as a source of heat generation and finding out temperature by thermal analysis [3-13]. However, this analysis was mainly done for single phase bus bar arrangement. In this thesis, the same principle is implemented for four metals viz. Aluminium 6063, Stainless steel, Mild steel, Aluminium AlMgSi. and for three phase bus bar arrangement as well. The temperature rise for each of these four metals is found and the best one among them is selected.

Electric field near the spacer surface changes if there are any surface non linearities like hemispherical protrusions and depressions[14-17] or particles present near the spacer surface [18-21]. All of these defects were simulated using Finite Element Method for axisymmetric case. The electric field intensity undergoes an erratic change near the defect. The parameters of the defect like diameter, elevation was varied and the resulting changes in electric field intensity magnitude were noted.

Chapter 2

Electromagnetic and Thermal Analysis

2.1 Introduction

The maximum current that can be supplied by GIS is limited by the allowable temperature rise of the conductor and the enclosure. Hence, it is important from design point of view to estimate the temperature rise and its distribution across the GIS cross section, when a particular value of current flows through it. As per IEC 60517 C 23 for GIS temperature for conductors should be limited to 65^{o}C and for enclosures that are accessible, the temperature should be limited to 30^{o}C.

A particular value of AC steady state current is allowed to flow through the conductor and the losses occurring in the conductor and the enclosure are calculated through Magnetic Field Analysis using Ansoft Maxwell. These losses are then used as input to carry out the Thermal Analysis using Finite Element Method which predicts the temperature distribution across the GIS bus bar. Aluminium 6063, Aluminium AlMgsi, Stainless steel, Mild steel are considered as enclosure metals and conductor is made of Aluminium 6063.

2.2 Power Loss

The AC currrent flowing in the main conductor is time varying in nature, so is the magnetic flux due to it. To keep the flux constant, eddy currents are induced in the enclosure as shown in figure 2.2.1

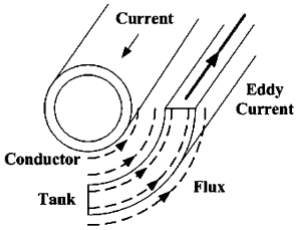

Figure 2.2.1: Eddy Currents in Single Phase GIS Bus Bar [6]

Power loss takes place in the main conductor due to AC steady state current flowing through it and in the enclosure due to eddy currents induced in it. So, the total loss occurring per unit length of GIS is calculated as

$$P = \int \frac{|\overline{J}|^2}{\sigma} dS \, (W / m) \tag{2.2.1}$$

$$\overline{J} = \overline{J_S} + \overline{J_E} \tag{2.2.2}$$

Where,
$\overline{J_S}$ = Source current density (A / m^2)
$\overline{J_E}$ = Eddy current density (A / m^2)
σ = Conductivity (Siemens / m)

2.2.1 Derivation of conductor power loss

The heat energy generated in any conducting material is

$$Heat = I^2 . R_{effective} . t \ \ Joules \tag{2.2.3}$$

where,
I = Current flowing through the conductor (A)
$R_{effective}$ = Effective resistance considering the skin effect (Ω)
t = time for which current is flowing (s)
Here, current of same value is passed for same amount of time. So, heat energy geneated depends directly on $R_{effective}$. i.e.

$$Heat \propto R_{effective} \tag{2.2.4}$$

Now,

$$R_{effective} = \frac{\rho . L}{A_{effective}} \tag{2.2.5}$$

where,
ρ= Resistivity of the material (Ω . m)

L= Length of the material (m)

$A_{effective}$ = Effective cross sectional area where current actually flows (m^2)

As, for the above studies, length is taken to be unity,

$$R_{effective} = \frac{\rho}{A_{effective}} \tag{2.2.6}$$

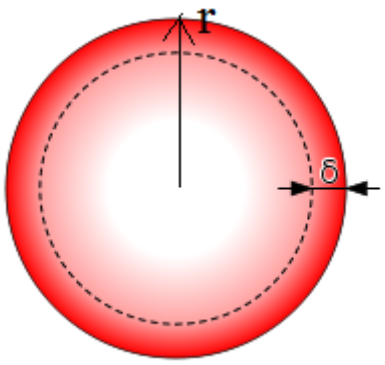

Figure 2.2.2: Skin depth

As shown in figure 2.2.2

$$A_{effective} = 2.\Pi.r.\delta \tag{2.2.7}$$

where,

r = Radius of the conductor (m)

δ = Skin depth (m)

From equation 2.2.6 and 2.2.7,

$$R_{effective} = \frac{\rho}{2.\Pi.r.\delta} \tag{2.2.8}$$

Now the value of r (radius of the conductor) is also constant for different materials. So,

$$R_{effective} \propto \frac{\rho}{\delta} \tag{2.2.9}$$

Now, skin depth is defined as

$$\delta = \sqrt{\frac{\rho}{\Pi.f.\mu}} \tag{2.2.10}$$

where,

ρ = Resistivity of the material (Ω . m)

f = Frequency of the current (Hz)

μ = Absolute magnetic permeability of the material (H / m)

From equation 2.2.9 and 2.2.10,

$$R_{effective} \propto \frac{\rho}{\sqrt{\frac{\rho}{\Pi \,.\, f \,.\, \mu}}} \tag{2.2.11}$$

Frequency (f) is constant at 50Hz. So, equation 2.2.11 simplifies to

$$R_{effective} \propto \sqrt{\rho \,.\, \mu} \tag{2.2.12}$$

So, losses produced in the main conductor are directly proportional to $\sqrt{\rho \,.\, \mu}$ of the material, as shown in equation 2.2.12

In this thesis, for simulation purpose, four metals can be used for making conductor part of GIS Bus bar as shown below in table 2.1

Table 2.1: Metals and Their Properties

Metal	$\rho(\Omega \,.m\,)$ x 10^{-8}	μ(H / m)	$\sqrt{\rho \,.\, \mu}$
Aluminium 6063	2.857	1	0.0001
Stainless Steel	90.9	1	0.0009
Mild Steel	14.3	100	0.0037
Aluminium AlMgSi	4.761	1	0.0002

As Aluminium 6063 has the lowest value of $\sqrt{\rho \,.\, \mu}$, it is used for main conductor simulation henceforth.

2.2.2 Derivation for enclosure power loss

As the conductor has large diameter, skin effect is taken into consideration. So, it's electrical cross sectional area (where current actually flows) i.e.$A_{effective}$is very small compared to it's physical cross sectional area.

In case of enclosure, its thickness being very small (in the order of few mm), skin effect is negligible. So, it's electrical cross sectional area (where current actually flows) i.e. $A_{effective}$is almost same as its physical area i.e. $\Pi \,.r^2$.

So, from equation 2.2.5,

$$R_{effective} = \frac{\rho \,.\, L}{\Pi \,.\, r^2} \tag{2.2.13}$$

For all types of materials considered, their lengths are kept constant and so are their radii. So, equation 2.2.13 simplifies to

$$R_{effective} \,\alpha\, \rho \tag{2.2.14}$$

So, from equation 2.2.14, losses produced in the enclosure are directly proportional to ρ(resistivity) of the enclosure material.

2.3 Thermal Analysis

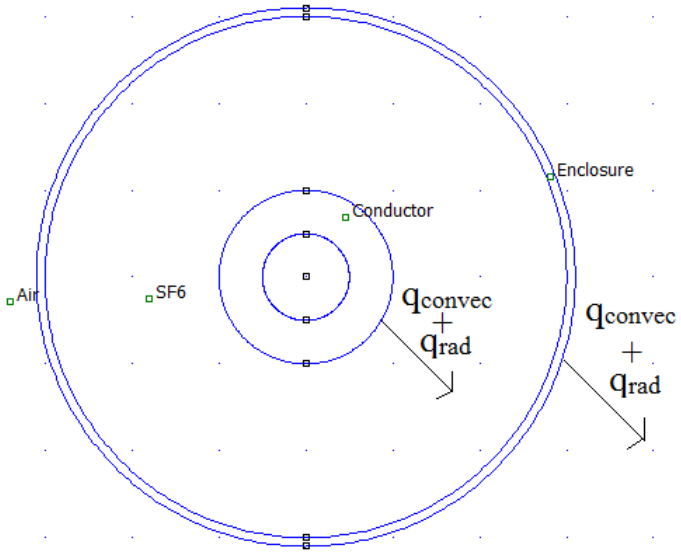

Figure 2.3.1: Heat Transfer Mechanism

The heat transfer inside GIS bus bar is shown in figure 2.3.1. Heat generated inside the conductor is transferred to the enclosure by SF_6 through convection and radiaition. The heat is generated inside the enclosure due to eddy currents through it. This heat and the heat coming from the conductor is transferred to the surrounding air.

2.3.1 Convection

Heat generated in the conductor is transferred to SF_6 through convection according to following equation.

$$q_{convec} = h_{convec} \,.\, A_s \,.\, (T_i - T_o) \tag{2.3.1}$$

where,

q_{convec}= Convection heat flow (W)

h_{convec} = Convection heat transfer coefficient (W / (m^2.K))

A_s = Surface area of conductor (m^2)

T_i = Conductor surface Temperature (K)

T_o = Temperature of SF_6 sufficiently away from conductor surface (K)

2.3.2 Radiation

The radiation heat transferred according to Stefan-Boltzman's law is defined as

$$q_{rad} = h_{rad} \,.\, A_s \,.\, (T_i - T_o) \tag{2.3.2}$$

where,
q_{rad} = Radiation heat flow (W)
$h_{rad} = \varepsilon.\sigma.$ (T_i+T_o) . (T_i^2 + T_o^2)
ε= Emissivity of the conductor surface
σ= Boltzman's Constant (W / m^2. K^4)
From equation 2.3.1 and 2.3.2 ,

$$q_{total} = h_{eff} \,.\, A_s \,.\, (T_i - T_o) \tag{2.3.3}$$

where,
h_{eff} (effective heat transfer coefficeint) = h_{convec}+ h_{rad}
Energy balance equation is

$$\nabla . \, q_{total} = Q - \rho \,.\, C \,.\, \frac{dT}{dt} \tag{2.3.4}$$

where,
q_{total} = Total heat flowing out (W)
Q = Total heat generated (due to conductor current) (W / m^3)
ρ = Density (Kg / m^3)
C = Specific heat capacity (J / Kg . K)

Above equation 2.3.4 is implemented by software across each mesh generated in FEM (Finite Element Method) Model, to get temperature distribution around of conductor surface.

Similar equation is solved across enclosure surface with T_i and T_o defined as temperature of enclosure and ambient temperature respectively.

2.4 Single Phase GIS bus bar Modeling

GIS bus bar is modeled as two concentric cylinders. The space between them is filled with SF_6 gas. The conductor is excited with current of 5000A (RMS). We are interested in temperature distribution across the cross sectional area of the bus bar. So, the Planar (2D) analysis is done by assuming the length of the bus bar to be unity i.e. one metre. Conductor is made of Aluminium 6063 and for making enclosure various metals like Aluminium 6063, Stainless steel, Mild steel, Aluminium AlMgSi are considered. The most suitable one among them is found

out by calculating the losses, temperature rise for each one of them , and then comparing the values so obtained.

2.4.1 Aluminium 6063 Enclosure

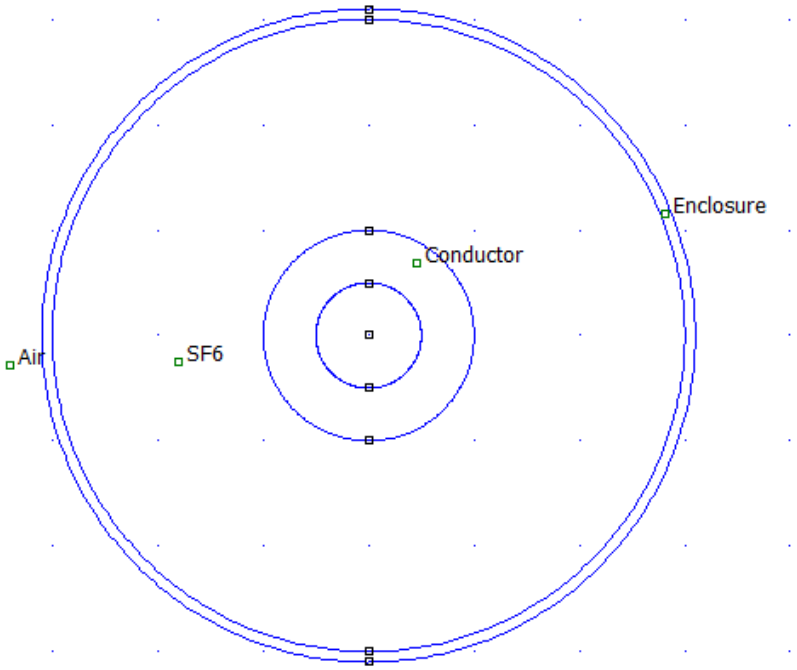

Figure 2.4.1: Single Phase GIS Bus Bar Arrangement

Aluminium 6063 is used for making both conductor and enclosure as shown in figure 2.4.1. The detailed dimensions and parameters are shown below in table 2.2

Table 2.2: Aluminium 6063 GIS Bus Bar Arrangement

Conductor (Aluminium 6063)		Enclosure (Aluminium 6063)	
Parameter	Value	Parameter	Value
inner radius (mm)	50	inner radius (mm)	300
outer radius (mm)	100	outer radius (mm)	310
thermal conductivity (W / m.K)	237.5	thermal conductivity (W / m.K)	237.5
electrical Conductivity (S / m)	35E+6	electrical Conductivity (S / m)	35E+6
specific heat (J / kg.K)	951	specific heat (J / kg.K)	951
density (kg / m^3)	2689	density (kg / m^3)	2689
50 Hz AC (A)	5000	50 Hz AC (A)	-

The bus bar is modeled in Ansoft with parameters as above and current of 5000A is set through the conductor.

The magnetic field intensity distribution obtained is shown in figure 2.4.2

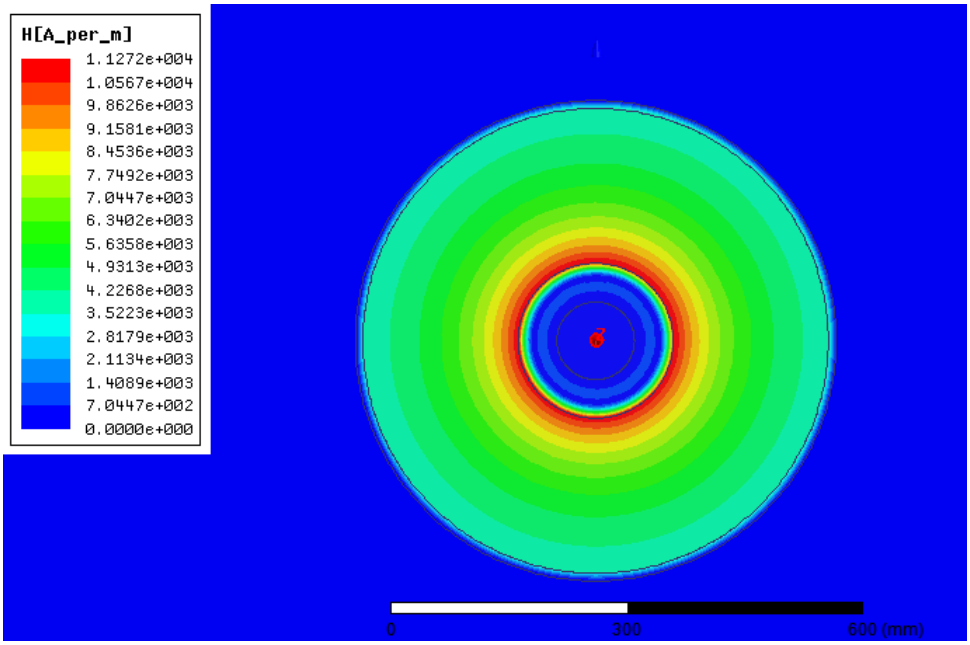

Figure 2.4.2: Magnetic Field Intensity Distribution

The current density distribution obtained is shown in figure 2.4.3

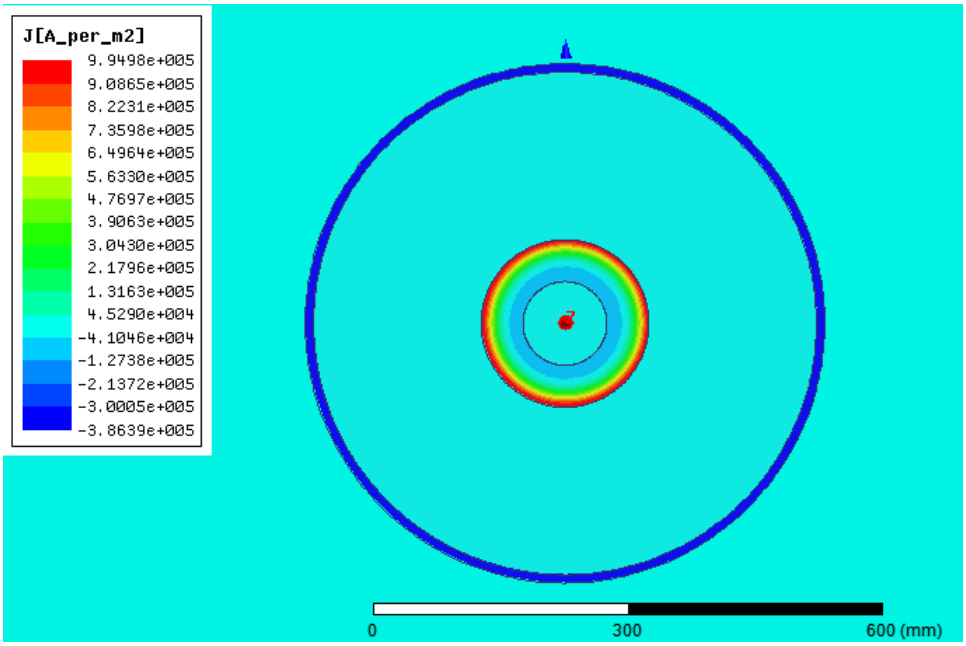

Figure 2.4.3: Current Density Distribution

Notice that conductor current is situated near the surface due to skin effect and the eddy current induced in the enclosure flows in opposite direction to source current, hence the negative value.

The values of losses generated in conductor and enclosure are as shown below in table 2.3. The losses taking place in conductor are due to source current and those in enclosure are due to eddy current induced.

Table 2.3: Power Losses Generated

Parameter	Conductor	Enclosure
Power Loss (W / m)	100.47	39.01

Material specification from table 2.1 and the loss values from table 2.2 are used as inputs for Finite Element Method (FEM) Model of the same bus bar and the temperature distribution is obtained as output, as shown in figure 2.4.4.

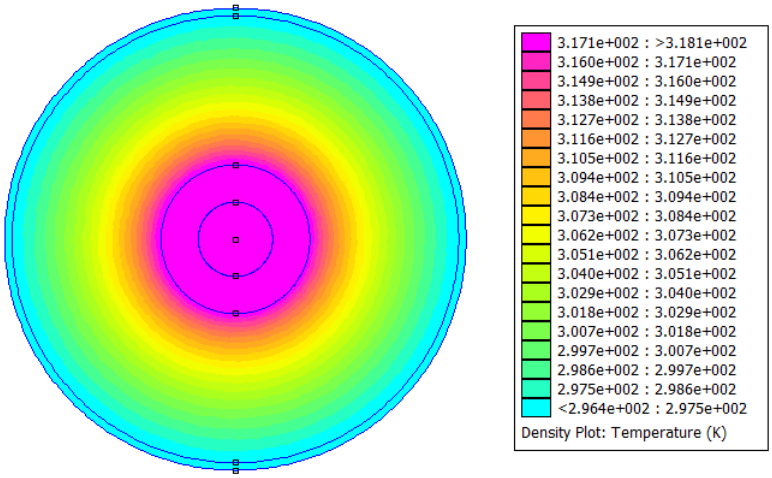

Figure 2.4.4: Temperature Distribution for Aluminium 6063 Enclosure

The specific temperatures are as shown in table 2.4

Table 2.4: Temperature for Aluminium 6063 Enclosure

Specification	Temperature (K)
Conductor	318.14
Enclosure	296.38
Ambient	294

2.4.2 Stainless Steel Enclosure

Conductor is made up of Aluminium 6063 and Stainless steel is used for making enclosure. The detailed dimensions and parameters are shown below in table 2.4

Table 2.5: Stainless Steel Enclosure GIS Bus Bar Arrangement

Conductor (Aluminium 6063)		Enclosure (Stainless Steel)	
Parameter	Value	Parameter	Value
inner radius (mm)	50	inner radius (mm)	300
outer radius (mm)	100	outer radius (mm)	310
thermal conductivity (W / m.K)	237.5	thermal conductivity (W / m.K)	43.2
electrical Conductivity (S / m)	35E+6	electrical Conductivity (S / m)	1.1E+6
specific heat (J / kg.K)	951	specific heat (J / kg.K)	460
density (kg / m^3)	2689	density (kg / m^3)	7850
50 Hz AC (A)	5000	50 Hz AC (A)	-

The values of losses generated in conductor and enclosure are as shown below in table 2.6

Table 2.6: Power Losses Generated

Parameter	Conductor	Enclosure
Power Loss (W / m)	100.47	1090.94

The temperature distribution is obtained in the similar way as shown in figure 2.4.5

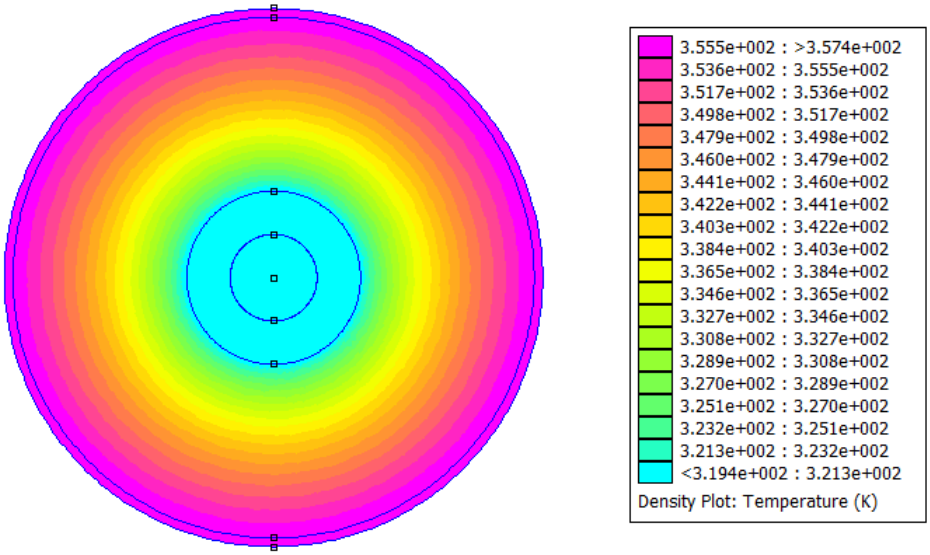

Figure 2.4.5: Temperature Distribution for Stainless Steel Enclosure

The temperature of enclosure is higher than that of the conductor as shown in figure 2.4.5 and the heat generated in enclosure flows inward.

The specific temperatures are as shown in table 2.6

Table 2.7: Temperature for Stainless Steel Enclosure

Specification	Temperature (K)
Conductor	319.41
Enclosure	357.42
Ambient	294

2.4.3 Mild Steel Enclosure

Conductor is made up of Aluminium 6063 and Mild steel is used for making enclosure. The detailed dimensions and parameters are shown below in table 2.8

Table 2.8: Mild Steel Enclosure GIS Bus Bar Arrangement

Conductor (Aluminium 6063)		Enclosure (Mild Steel)	
Parameter	Value	Parameter	Value
inner radius (mm)	50	inner radius (mm)	300
outer radius (mm)	100	outer radius (mm)	310
thermal conductivity (W / m.K)	237.5	thermal conductivity (W / m.K)	54
electrical Conductivity (S / m)	35E+6	electrical Conductivity (S / m)	6.99E+6
specific heat (J / kg.K)	951	specific heat (J / kg.K)	490
density (kg / m^3)	2689	density (kg / m^3)	7850
50 Hz AC (A)	5000	50 Hz AC (A)	-

The values of losses generated in conductor and enclosure are as shown below in table 2.9

Table 2.9: Power Losses Generated

Parameter	Conductor	Enclosure
Power Loss (W / m)	100.47	702.89

The temperature distribution is obtained in the similar way as shown in figure 2.4.6

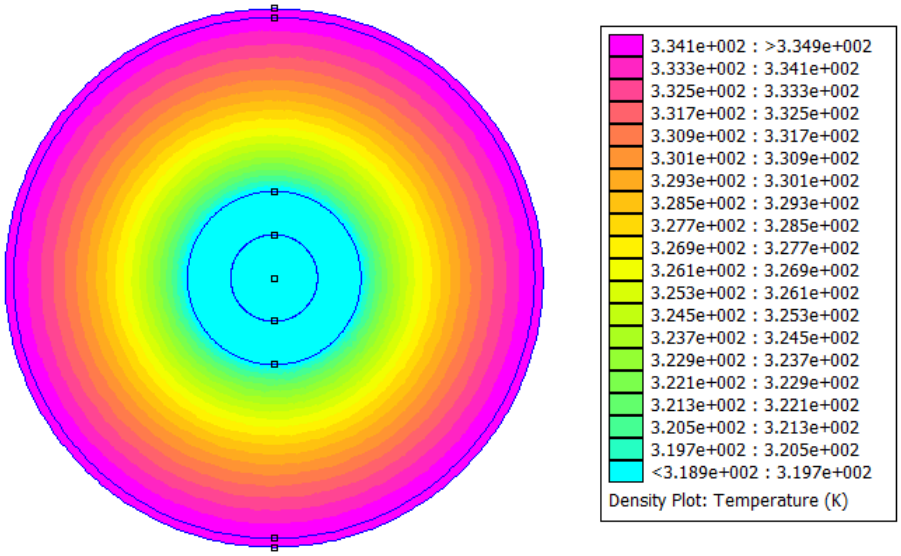

Figure 2.4.6: Temperature Distribution for Mild Steel Enclosure

The specific temperatures are as shown in table 2.10

Table 2.10: Temperature for Mild Steel Enclosure

Specification	Temperature (K)
Conductor	318.94
Enclosure	334.90
Ambient	294

2.4.4 Aluminium AlMgSi Enclosure

Conductor is made up of Aluminium 6063 and Aluminium AlMgSi is used for making enclosure. The detailed dimensions and parameters are shown below in table 2.11

Table 2.11: Aluminium AlMgSi Enclosure GIS Bus Bar Arrangement

Conductor (Aluminium 6063)		Enclosure (Aluminium AlMgSi)	
Parameter	Value	Parameter	Value
inner radius (mm)	50	inner radius (mm)	300
outer radius (mm)	100	outer radius (mm)	310
thermal conductivity (W / m.K)	237.5	thermal conductivity (W / m.K)	210
electrical Conductivity (S / m)	35E+6	electrical Conductivity (S / m)	21E+6
specific heat (J / kg.K)	951	specific heat (J / kg.K)	900
density (kg / m^3)	2689	density (kg / m^3)	2700
50 Hz AC (A)	5000	50 Hz AC (A)	-

The values of losses generated in conductor and enclosure are as shown below in table 2.12

Table 2.12: Power Losses Generated

Parameter	Conductor	Enclosure
Power Loss (W / m)	100.47	63.35

The temperature distribution is obtained in the similar way as shown in figure 2.4.7

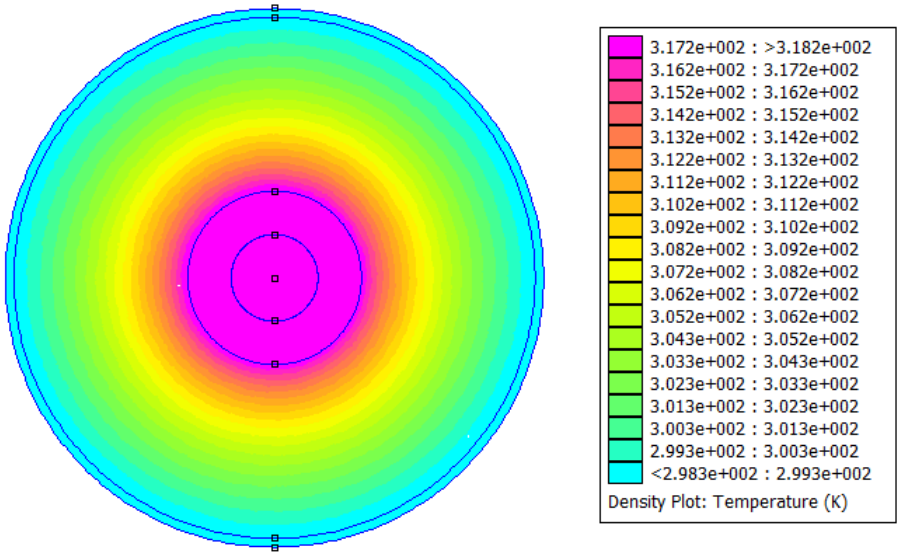

Figure 2.4.7: Temperature Distribution for AlMgSi Enclosure

The specific temperatures are as shown in table 2.12

Table 2.13: Temperature for AlMgSi Enclosure

Specification	Temperature (K)
Conductor	318.18
Enclosure	298.28
Ambient	294

2.4.5 Summary of Single Phase Enclosures

Table 2.14: Loss values and resistivity of enclosure material (ρ)

Enclosure Metal	resistivity (ρ) (Ω. m) x 10^{-8}	Electrical Loss in enclosure (W / m)
Aluminium 6063	2.857	39.01
Stainless Steel	90.9	1090.94
Mild Steel	14.30	702.89
Aluminium AlMgSi	4.761	63.35

Table 2.14 shows that losses in enclosure depend upon resistivity of enclosure metal (ρ) (Ω. m) as shown in 2.2.2

2.5 Three Phase GIS bus bar Modeling

Actual three phase GIS bus bar is modeled as shown in figure 2.5.1. Three phase conductors are separated by spacer in the middle and the remaining volume is filled with SF6 gas.The spacing between them is 300 mm. The phase conductors are excited with current of 5000A (RMS) and the losses and the temperature distribution is calculated as above.

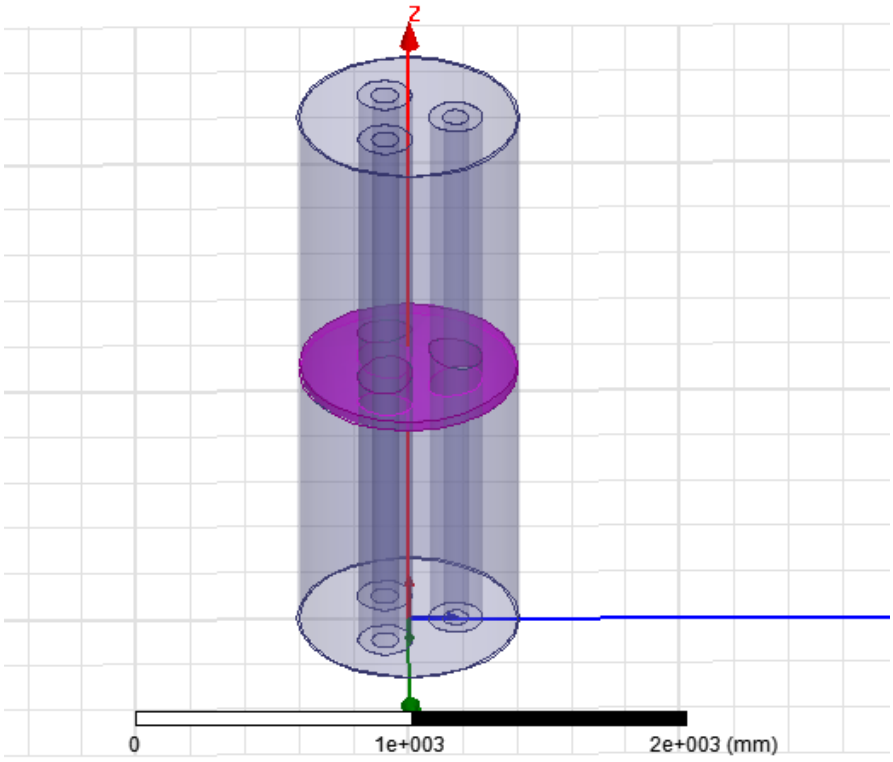

Figure 2.5.1: Actual Three Phase GIS Bus Bar Arrangement

2.5.1 Aluminium 6063 Enclosure

The planar (2D) model used for power loss and temperature calculations is shown in figure 2.5.2

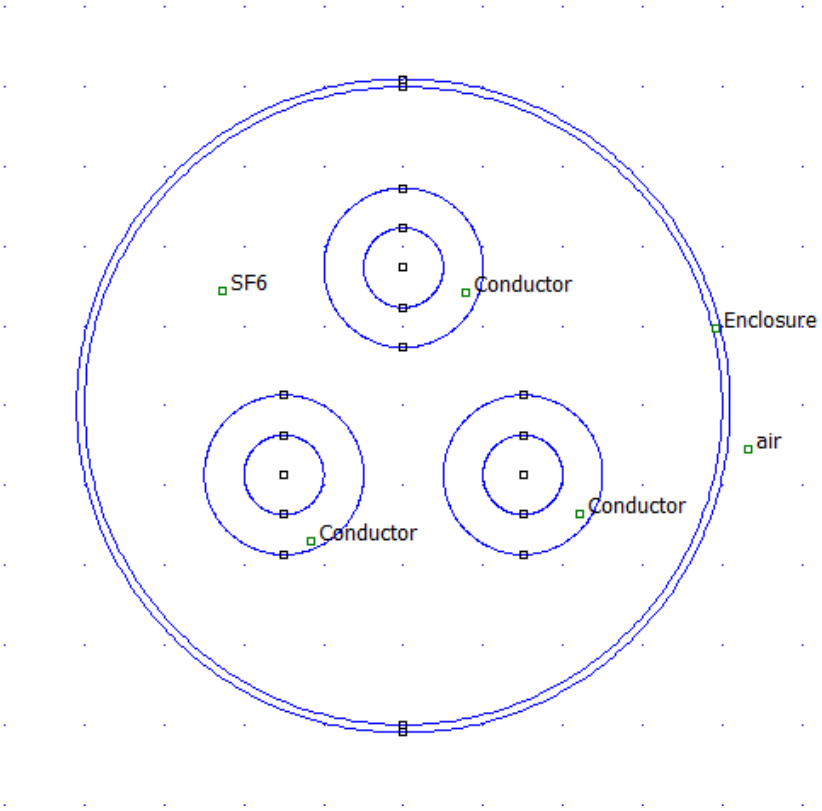

Figure 2.5.2: Planar (2D)Three Phase GIS Bus Bar Arrangement

The detailed dimensions and parameters are as given in table 2.15

Table 2.15: Aluminium 6063 Enclosure GIS Bus Bar Arrangement

Conductor (Aluminium 6063)		Enclosure (Aluminium 6063)	
Parameter	Value	Parameter	Value
inner radius (mm)	50	inner radius (mm)	400
outer radius (mm)	100	outer radius (mm)	410
thermal conductivity (W / m.K)	237.5	thermal conductivity (W / m.K)	237.5
electrical Conductivity (S / m)	35E+6	electrical Conductivity (S / m)	35E+6
specific heat (J / kg.K)	951	specific heat (J / kg.K)	951
density (kg / m^3)	2689	density (kg / m^3)	2689
50 Hz AC (A)	5000	50 Hz AC (A)	-

The values of losses generated in three phase conductors are same as they are excited with the same magnitude of current. The losses taking place in the conductors and the enclosure are as shown in table 2.16

Table 2.16: Power Losses Generated

Parameter	Each Phase Conductor	Enclosure
Power Loss (W / m)	113.60	44.18

The temperature distribution is obtained in the similar way as shown in figure 2.5.3

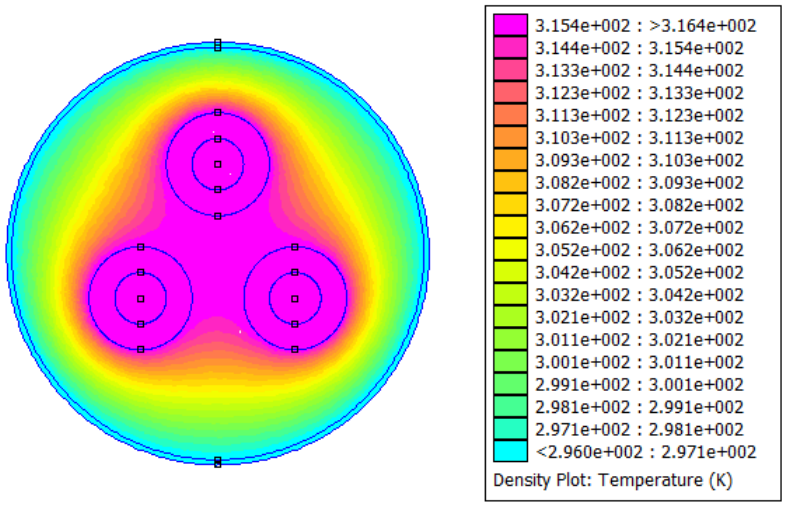

Figure 2.5.3: Temperature Distribution for Aluminium 6063 Enclosure

The specific temperatures are as shown in table 2.17

Table 2.17: Temperature for Aluminium 6063

Specification	Temperature (K)
Each Phase Conductor	316.38
Enclosure	296.4
Ambient	294

2.5.2 Stainless Steel Enclosure

Phase conductors are made up of Aluminium 6063 and Stainless steel is used for making enclosure. The detailed dimensions and parameters are shown below in table 2.18

Table 2.18: Stainless Steel Enclosure GIS Bus Bar Arrangement

Conductor (Aluminium 6063)		Enclosure (Stainless Steel)	
Parameter	Value	Parameter	Value
inner radius (mm)	50	inner radius (mm)	400
outer radius (mm)	100	outer radius (mm)	410
thermal conductivity (W / m.K)	237.5	thermal conductivity (W / m.K)	43.2
electrical Conductivity (S / m)	35E+6	electrical Conductivity (S / m)	1.1E+6
specific heat (J / kg.K)	951	specific heat (J / kg.K)	460
density (kg / m^3)	2689	density (kg / m^3)	7850
50 Hz AC (A)	5000	50 Hz AC (A)	-

The values of losses generated in conductor and enclosure are as shown below in table 2.19

Table 2.19: Power Losses Generated

Parameter	Each Phase Conductor	Enclosure
Power Loss (W / m)	128.55	393.87

The temperature distribution is obtained in the similar way as shown in figure 2.5.4

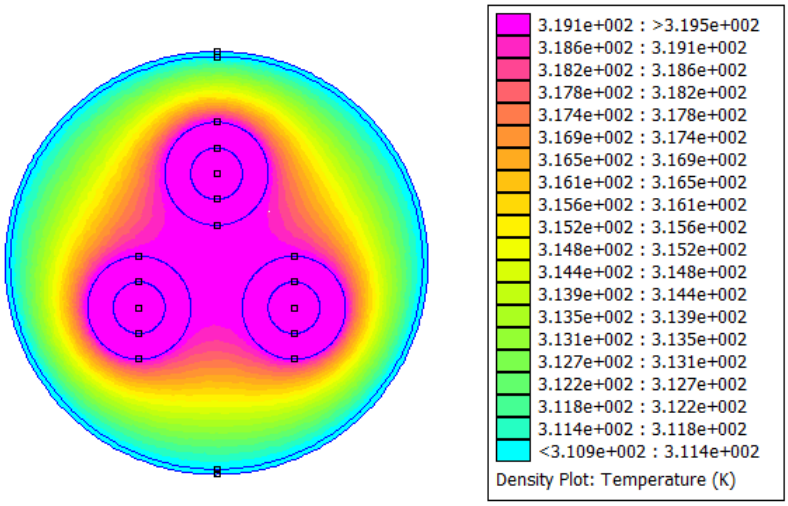

Figure 2.5.4: Temperature Distribution for Stainless Steel Enclosure

The specific temperatures are as shown in table 2.20

Table 2.20: Temperature for Stainless Steel

Specification	Temperature (K)
Each Phase Conductor	319.49
Enclosure	310.94
Ambient	294

2.5.3 Mild Steel Enclosure

Phase conductors are made up of Aluminium 6063 and Mild Steel is used for making enclosure. The detailed dimensions and parameters are shown below in table 2.21

Table 2.21: Mild Steel Enclosure GIS Bus Bar Arrangement

Conductor (Aluminium 6063)		Enclosure (Mild Steel)	
Parameter	Value	Parameter	Value
inner radius (mm)	50	inner radius (mm)	400
outer radius (mm)	100	outer radius (mm)	410
thermal conductivity (W / m.K)	237.5	thermal conductivity (W / m.K)	54
electrical Conductivity (S / m)	35E+6	electrical Conductivity (S / m)	6.99E+6
specific heat (J / kg.K)	951	specific heat (J / kg.K)	490
density (kg / m^3)	2689	density (kg / m^3)	7850
50 Hz AC (A)	5000	50 Hz AC (A)	-

The values of losses generated in conductor and enclosure are as shown below in table 2.22

Table 2.22: Power Losses Generated

Parameter	Each Phase Conductor	Enclosure
Power Loss (W / m)	128.22	304.18

The temperature distribution is obtained in the similar way as shown in figure 2.5.5

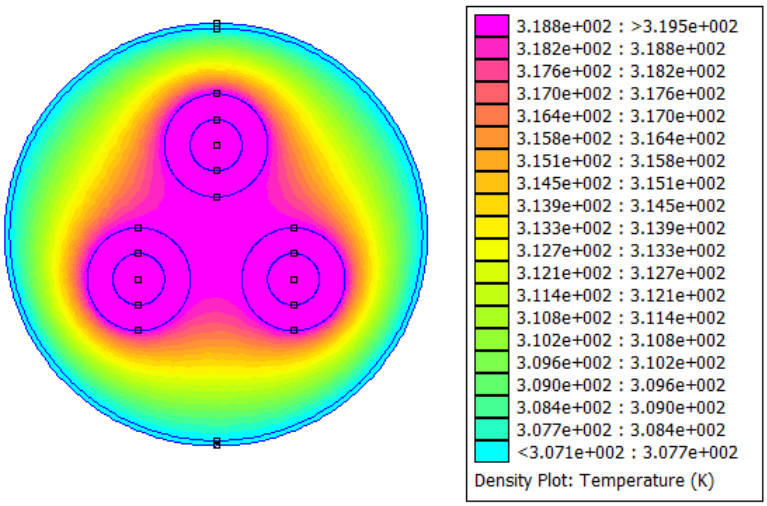

Figure 2.5.5: Temperature Distribution for Mild Steel Enclosure

The specific temperatures are as shown in table 2.23

Table 2.23: Temperature for Mild Steel

Specification	Temperature (K)
Each Phase Conductor	319.45
Enclosure	307.12
Ambient	294

2.5.4 Aluminium AlMgSi Enclosure

Phase conductors are made up of Aluminium 6063 and Aluminium AlMgSi is used for making enclosure. The detailed dimensions and parameters are shown below in table 2.24

Table 2.24: Aluminium AlMgSi GIS Enclosure Bus Bar Arrangement

Conductor (Aluminium 6063)		Enclosure (Aluminium AlMgSi)	
Parameter	Value	Parameter	Value
inner radius (mm)	50	inner radius (mm)	400
outer radius (mm)	100	outer radius (mm)	410
thermal conductivity (W / m.K)	237.5	thermal conductivity (W / m.K)	210
electrical Conductivity (S / m)	35E+6	electrical Conductivity (S / m)	21E+6
specific heat (J / kg.K)	951	specific heat (J / kg.K)	900
density (kg / m^3)	2689	density (kg / m^3)	2700
50 Hz AC (A)	5000	50 Hz AC (A)	-

The values of losses generated in conductor and enclosure are as shown below in table 2.25

Table 2.25: Power Losses Generated

Parameter	Each Phase Conductor	Enclosure
Power Loss (W / m)	113.60	71.28

The temperature distribution is obtained in the similar way as shown in figure 2.5.6

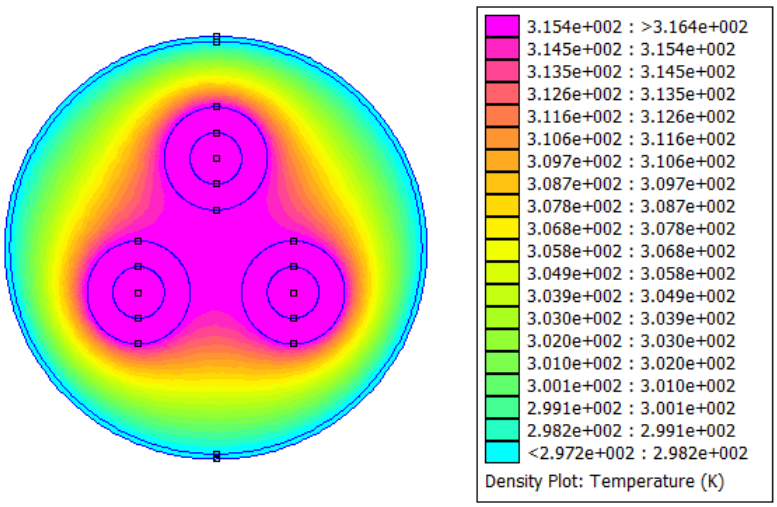

Figure 2.5.6: Temperature Distribution for AlMgSi Enclosure

The specific temperatures are as shown in table 2.26

Table 2.26: Temperature for Aluminium AlMgSi

Specification	Temperature (K)
Each Phase Conductor	316.39
Enclosure	297.19
Ambient	294

2.6 Summary

In case of three phase bus bar, the temperature of the phase conductors is almost constant and varies slightly with the material used for making enclosure, as shown in table 2.27.

Table 2.27: Temperatures for various Metals

Metal	Three Phase Temperature (K)	
	Conductor	Enclosure
Aluminium 6063	316.38	296.04
Aluminium AlMgSi	316.39	297.19
Stainless Steel	319.45	310.94
Mild Steel	759.52	307.12

Chapter 3

Electric Field Near The Spacer Surface Without Any Defects

The spacer surface is considered for electric field studies, even in case of healthy spacer (without any surface defects and/or particles) , because of following prominent reasons.

1. Weak Covalent Bond : The electrons near the spacer surface experience weak attractive forces than those well inside the spacer. So, these surface electrons may break the bonds and contribute to increased conductivity and partial discharge incidences along the spacer surface.

2. Non-uniformity : The spacer surface may appear smooth from outside,but it is made up of large number of sharp points which may cause local field enhancement and thereby partial discharge.

The spacers are mainly of two shapes viz. disc and conical. Disc type spacers are considered for further studies.

3.1 Disc Type Spacer

The component of GIS considered for the study is shown in figure 3.1.1. It is composed of inner and outer conductors separated by spacer. ro is the radius of inner electrode and R the radius of the outer electrode. Zs is the spacer's half thickness at the inner electrode and Ze is the same at the outer electrodes. The calculations can be done in P.U. values considering applied voltage as base voltage and ro as the base for length. The electric field in P.U. values can be calculated using equation 3.1.1

$$E_{PU} = \left({}^{E}computed/{}^{V}applied\right) * ro \tag{3.1.1}$$

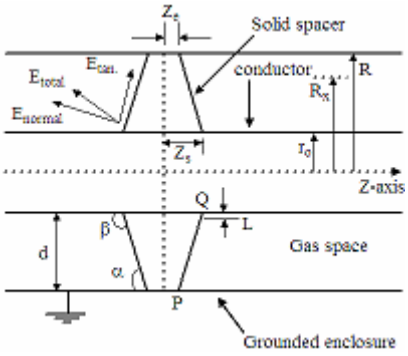

Figure 3.1.1: Spacer Electrode Arrangement in GIS [15]

The voltage applied to inner electrode is 100 kV and outer electrode is grounded. The value of ro is 10 cm.The spacer's dimensions and its relative permittivity value was maintained fixed as Ze, Zs, R and εr : 0.2, 1, 3 p.u. and 6 respectively.

The FEM (2D) model of the spacer is shown in figure 3.1.2 and the actual 3D model is 3.1.3

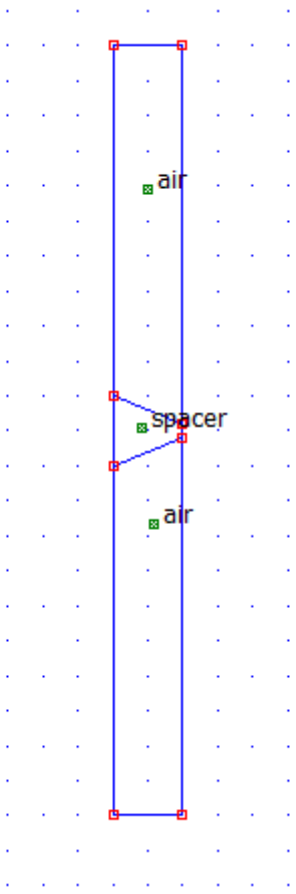

Figure 3.1.2: Spacer FEM (2D) model

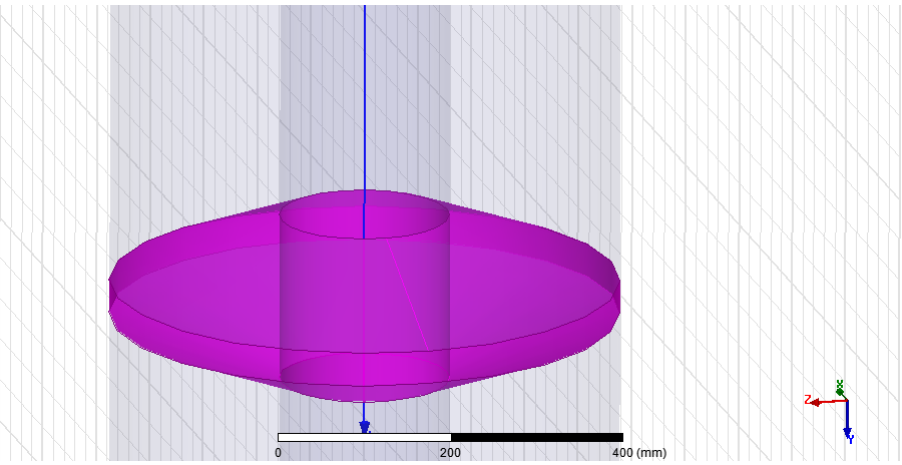

Figure 3.1.3: Spacer Maxwell (3D) Model

The electric field along the spacer surface as observed from FEM model is shown in figure 3.1.4

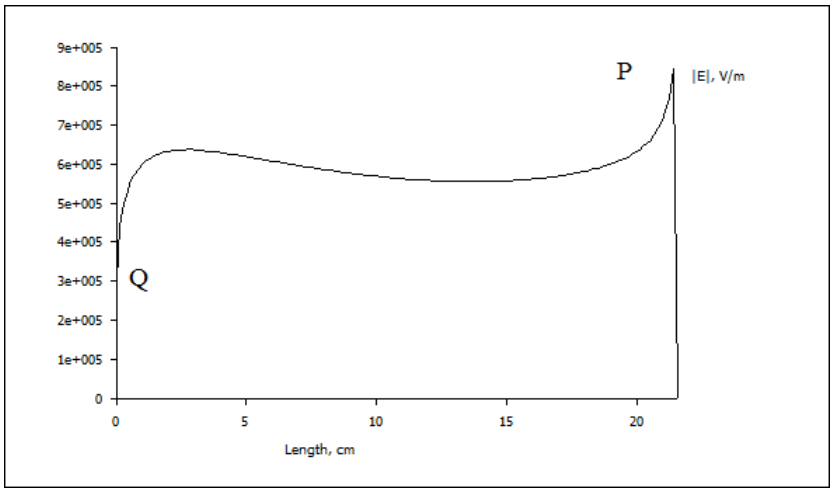

Figure 3.1.4: Electric Field Along the Spacer Surface Using 2D Modeling

The electric field at points P and Q follows a particular equation as given in 3.1.2 [2] . Here, L is the distance from the inner conductor surface, d is a constant quantity defined as $d = R - r_o$ i.e. the separation between inner and outer conductors, k a constant value. The value of m depends upon spacer's permittivity and inclination angle α.

$$E = k\left(\frac{L}{d}\right)^m \tag{3.1.2}$$

The value of m is negative near point P and positive near point Q. So, the electric field is very low near point Q and very high near point P. The variation of electric field near points P and Q is as shown in figure 3.1.4

Similarly, the electric field along the same surface using 3D studies is shown in figure 3.1.5.

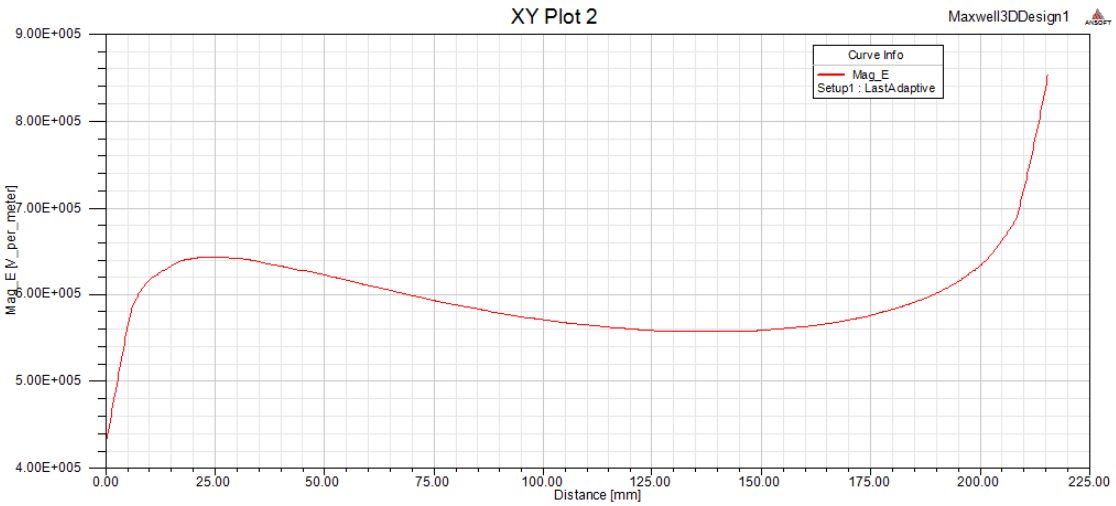

Figure 3.1.5: Electric Field along the spacer using 3D Modeling

Electric field along the surface without any defects is same as calculated from 2D and 3D studies.

The equipotential lines and the electric field density as found out from FEM are as shown in figure 3.1.6

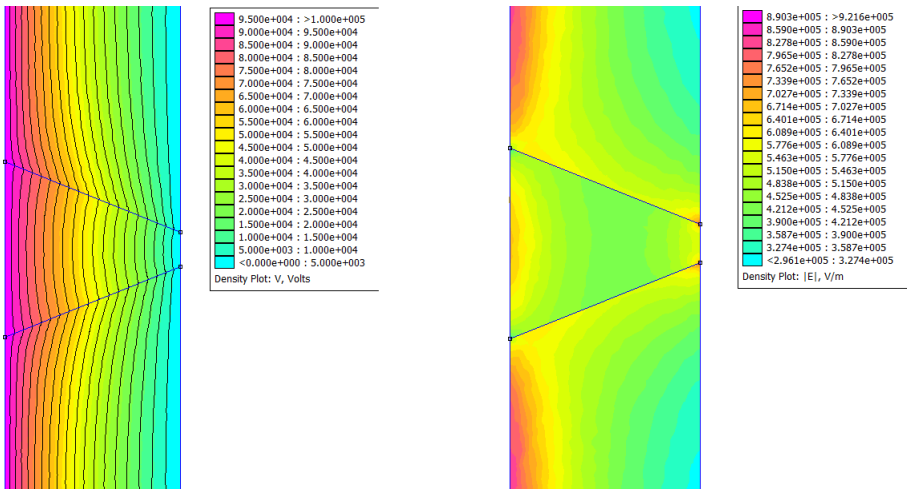

Figure 3.1.6: Equipotential Lines & Electric Field Intensity

Chapter 4

Electric Field Near The Spacer Surface With Defects

Spacers are used to isolate conducting part from the ground. The surface of the spacers may become non uniform due to the improper manufacturing. The conducting and non conducting particles also get generated due to mechanical abrasions and arcing taking place during the operation of isolating switches and circuit breakers. Such surface non uniformity and particles present near the spacer surface make it vulnerable to electric breakdown. So, it is important to study the effect of variations in size, type and location of the surface non-uniformity and free particles close to the spacer surface on the electric field distribution near the spacer gas interface.

Finite Element Method (FEM) has been used to study the electric field distribution near the spacer surface considering the above mentioned surface defects and particles.

These defects may be classified into following categories.

1. Protrusions
2. Depressions
3. Flying Particles
4. Adhered particles

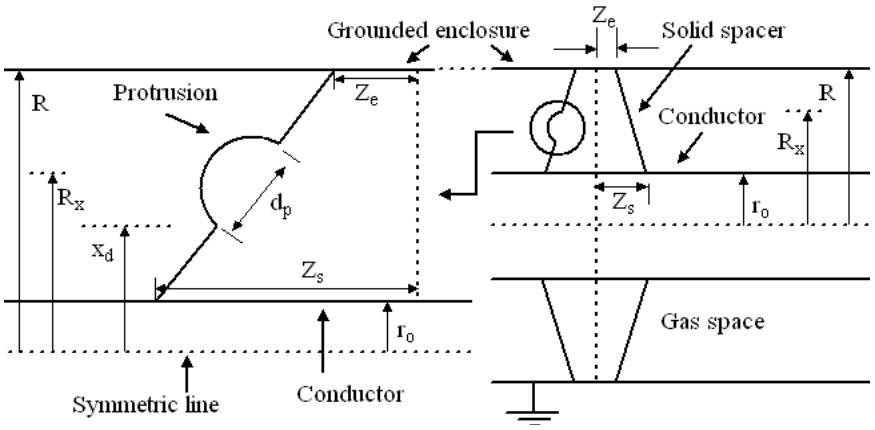

Figure 4.0.1: Hemisphere Protrusion Defect [15]

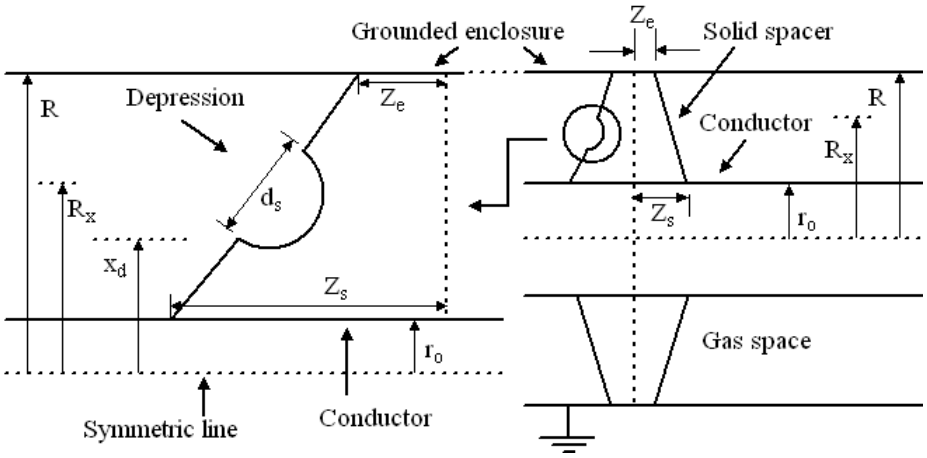

Figure 4.0.2: Hemisphere Depression Defect [15]

These defects viz. protrusion and depression, depicted by figure 4.0.1 and figure 4.0.2 respectively, can be modeled by considering concave and convex hemisphere of varying radius and position on the spacer surface.

These defects are characterisied by d_p, d_s and x_d. Here, d_p is the protrusion's diameter and d_s is depression's diameter. x_d shows defect's radial position.

Defect Field Factor (DFF) is defined as the ratio between the electric field value with the defect present and the electric field value with no defect, at the same location.

4.1 Protrusion

The equipotential lines in case of protrusion are as shown in figure 4.1.1

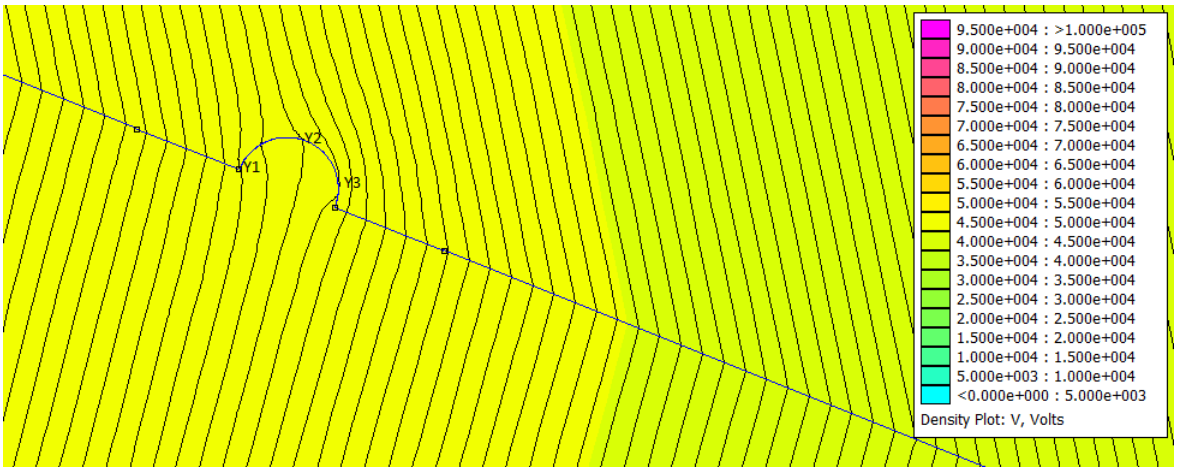

Figure 4.1.1: Equipotential Lines near Protrusion

and the corroesponding electric field distribution in figure 3.1.2

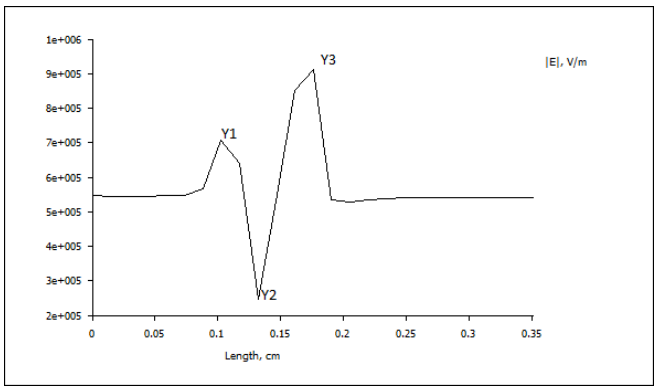

Figure 4.1.2: Electric Field with Protrusion d_p= 1mm

Electric Field Intensity is defined as $E = -\frac{dV}{dX}$. It explains the the peaks in electric field at points Y_1 and Y_3 and dip in electric field at point Y_2.

4.1.1 Electric Field Changes With Variation in Protrusion Diameter

The radial position of the protrusion is kept fixed at x_d= 2 p.u. and the diameter of the hemisphere is varied as 2mm, 1.5mm, 1mm, 0.5mm.The electric field along the spacer surface for the respective cases are shown.

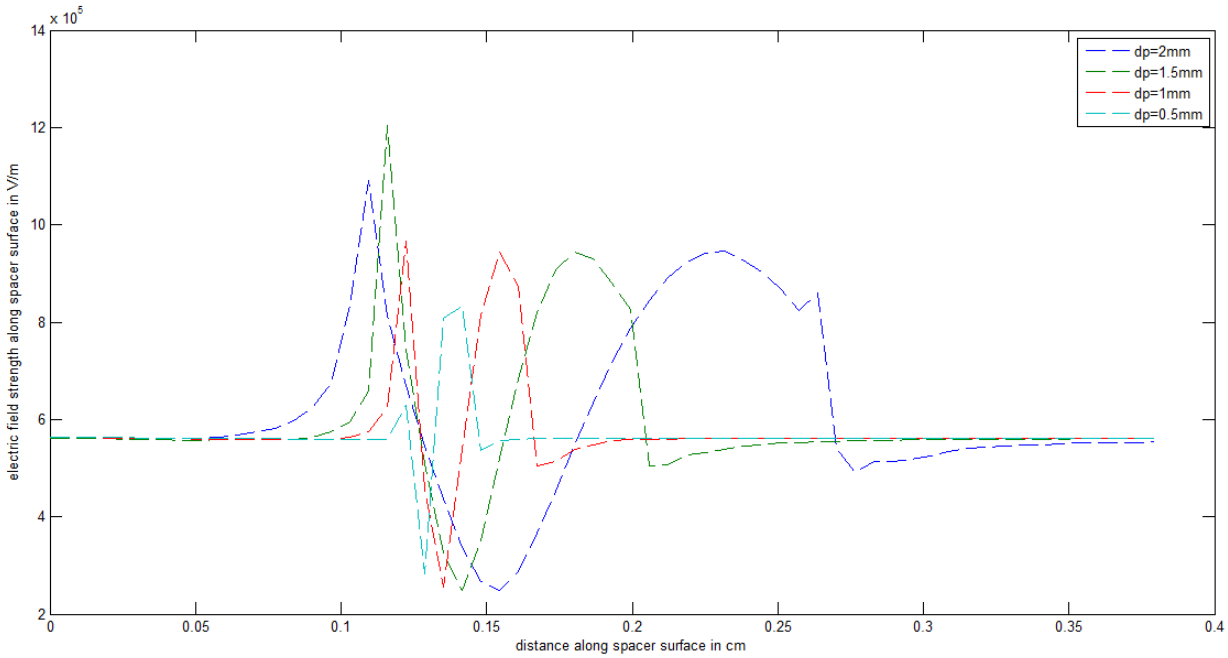

Figure 4.1.3: Electric Field with Diameter Variations

The electric field gets disturbed at the location of protrusion and disturbance persists only for the length of protrusion i.e. As diameter decreases, DFF decreases.

Table 4.1: DFF variation with Protrusion Diameter Variation

Diameter of Protrusion	Defect Field Factor (DFF)
2mm	1.83
1.5mm	2
1mm	1.6
0.5mm	1.3

4.1.2 Electric Field Changes With Variation in Protrusion Radial Location

The diameter of the protrusion is kept fixed at d_p= 1mm and their radial positions are varied as 1.1pu, 1.5pu, 2pu, 2.5pu, 2.9pu. The electric field along the spacer surface for the respective cases is shown

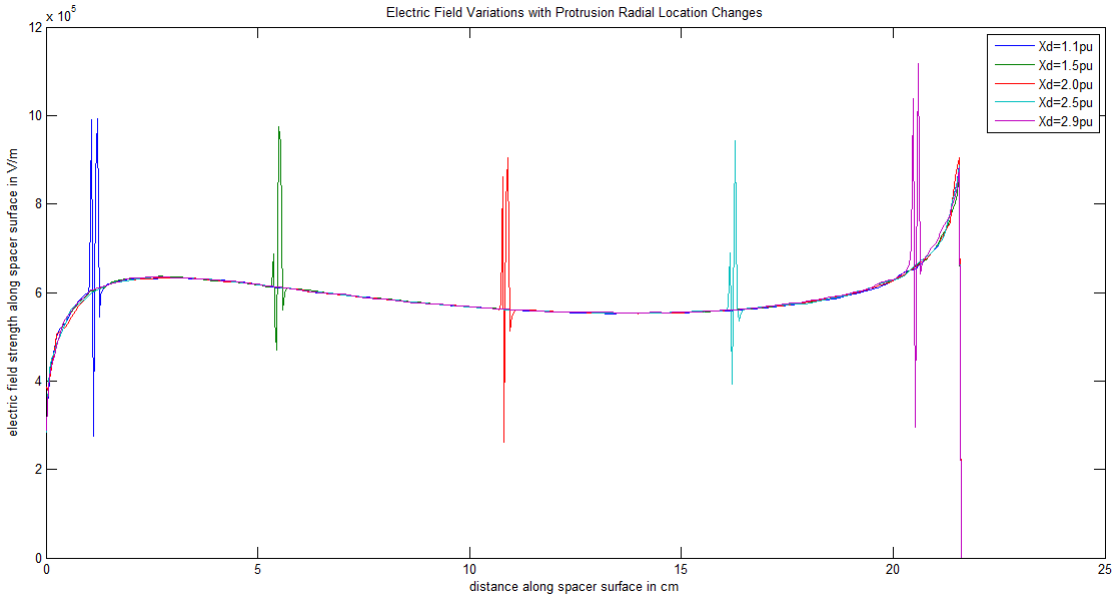

Figure 4.1.4: Electric Field Variation with Protrusion Radial Location Changes

DFF = 1.6 and is almost independent of location of protrusion.

4.2 Depression

The equipotential lines in case of depression are as shown in figure 4.2.1

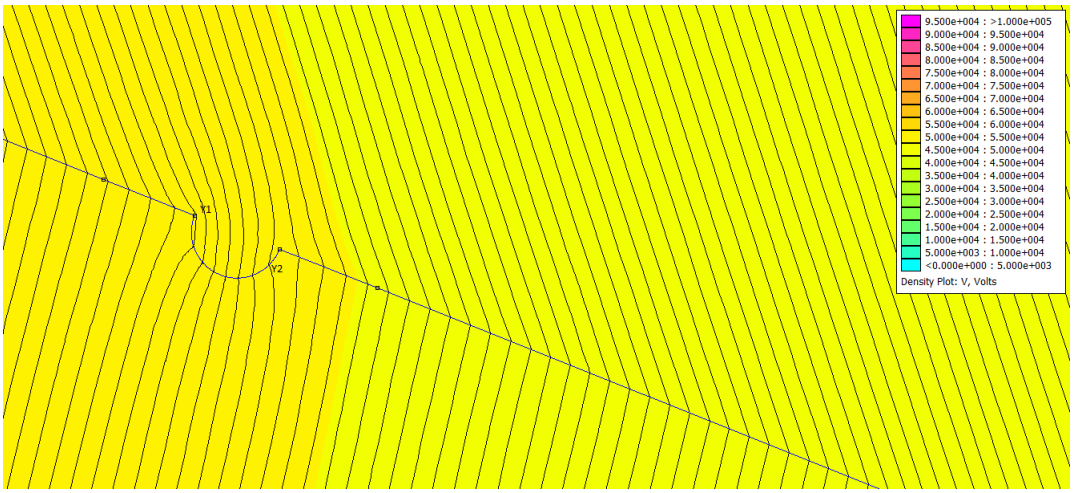

Figure 4.2.1: Equipotential Lines near Depression

and the corroesponding electric field distribution in figure 3.2.2

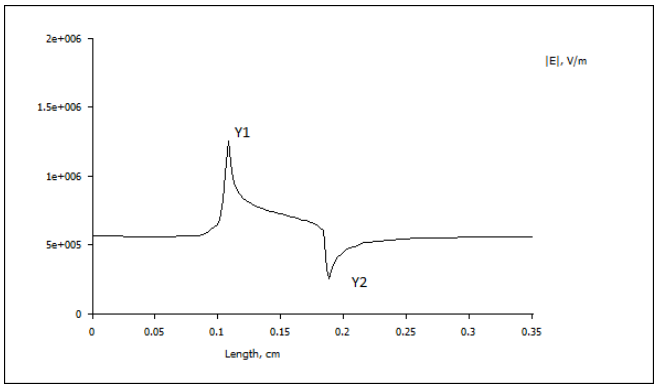

Figure 4.2.2: Electric Field Distribution with d_s=1mm

Electric Field Intensity is defined as $E = -\frac{dV}{dX}$. It explains the the peaks in electric field at point Y_1 and dip in electric field at point Y_2

4.2.1 Electric Field Changes With Variation in Depression Diameter

The radial position of the depression is kept fixed at x_d= 2 p.u. and the diameter of the hemisphere is varied as 2mm, 1.5mm, 1mm, 0.5mm.The electric field along the spacer surface for the respective cases is shown

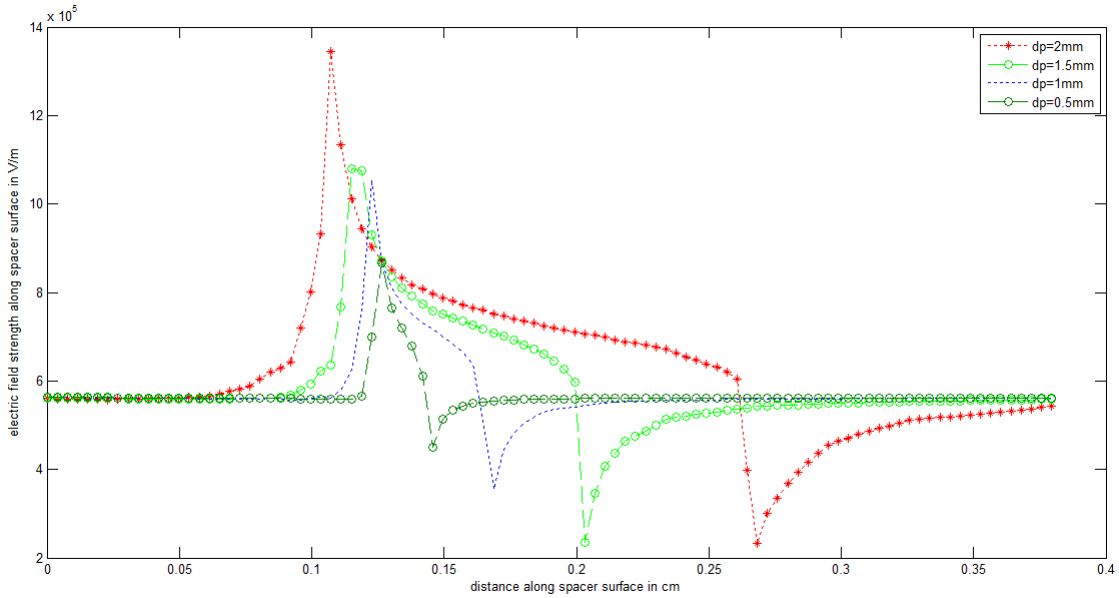

Figure 4.2.3: Electric Field with Depression Diameter Variation

The electric field gets disturbed at the location of depression and disturbance persists only for the length of depression i.e. As diameter decreases, DFF decreases.

Table 4.2: DFF variation with Depression Diameter Variation

Diameter of Depression	Defect Field Factor (DFF)
2mm	2.2
1.5mm	1.8
1mm	1.6
0.5mm	1.4

4.2.2 Electric Field Changes With Variation in Depression Radial Location

The diameter of the depression is kept fixed at d_s= 1mm and their radial positions are varied as 1.1pu, 1.5pu, 2pu, 2.5pu, 2.9pu. The electric field along the spacer surface for the respective cases is shown

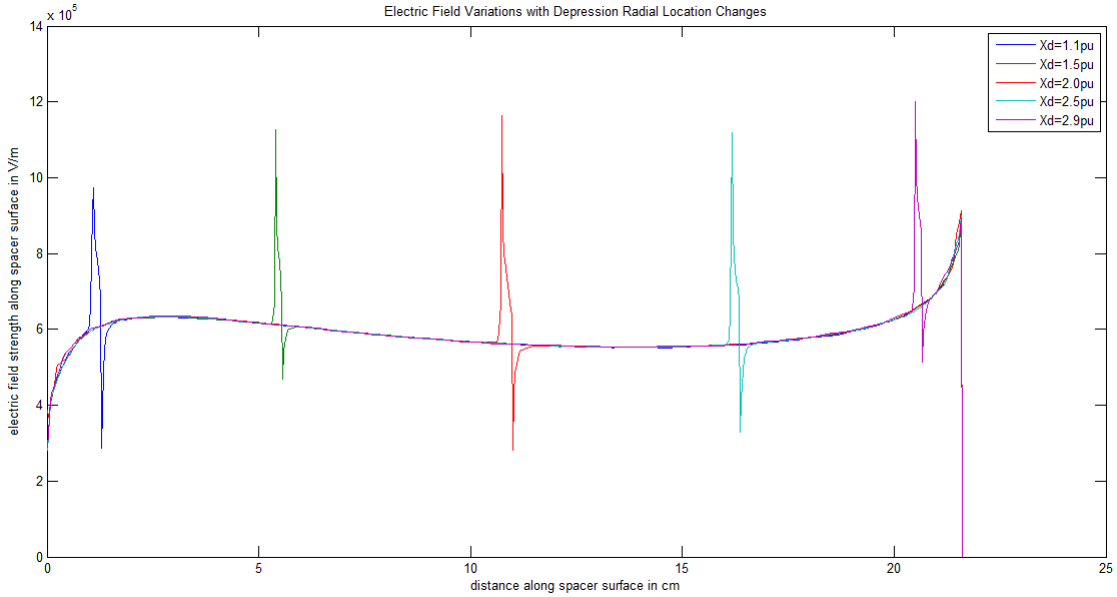

Figure 4.2.4: Electric Field Variation with Depression Radial Location Changes

DFF = 1.6 and is almost independent of location of protrusion

4.3 Flying Particles

The flying particles near the spacer surface are as shown in figure 4.3.1

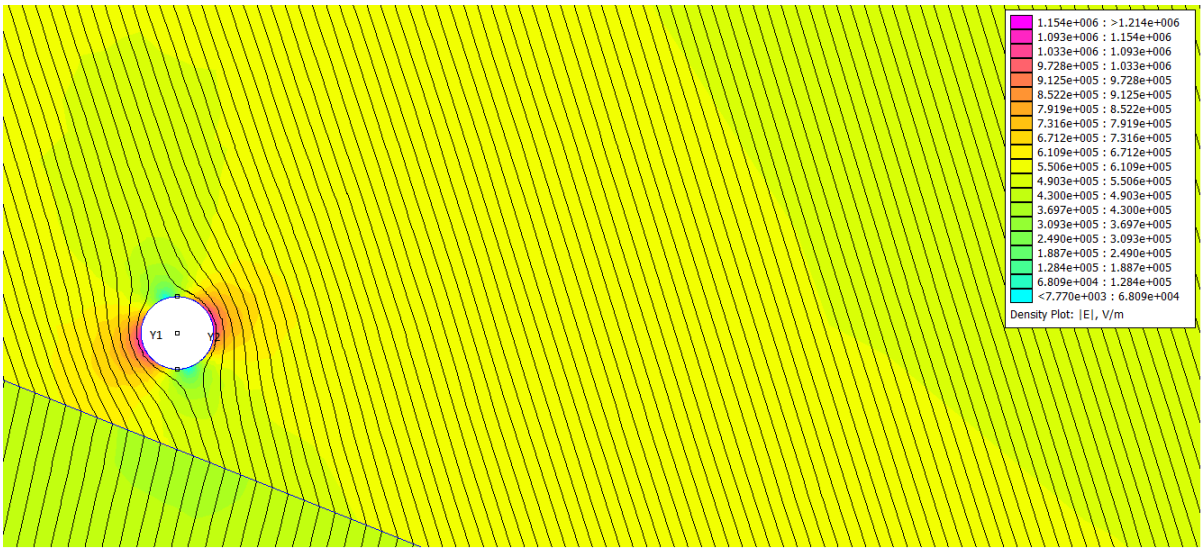

Figure 4.3.2: Equipotential Line Near Flying Particle

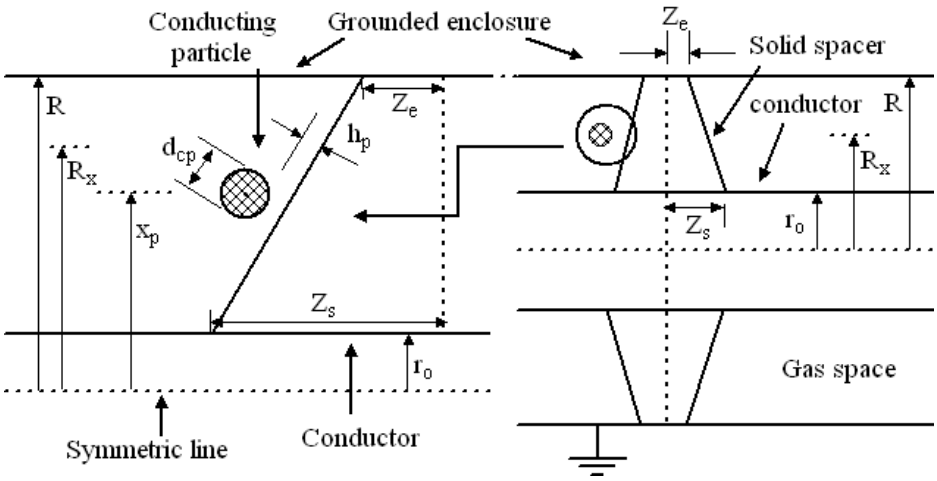

Figure 4.3.1: Flying Particle Near Spacer Surface [15]

The flying particles are modeled by three variables as d_{cp}, h_p, x_p. Here, d_{cp} is the diameter of the flying particle, h_p the elevation between the particle and the spacer surface and x_p the radial location of the particle.

The equipotential lines in case of flying particle are shown in figure 4.3.2 and corroesponding electric field distribution near the spacer surface is as shown in figure 4.3.3

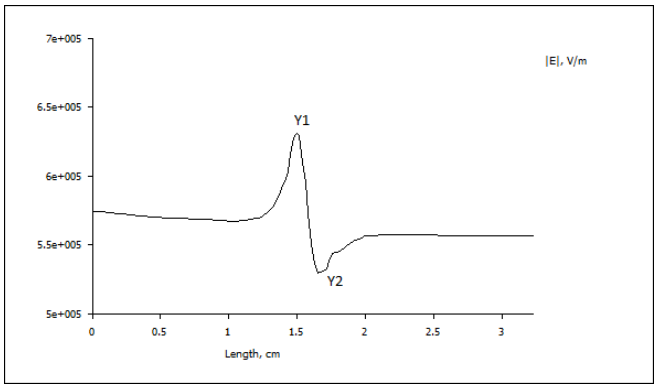

Figure 4.3.3: Electric Field With Flying Particle d_{cp}= 1mm

The conducting particle disturbs the electric field distribution around the spacer and charge redistribution takes place in such a way that electric field inside the particle is zero and surface of the particle forms an equipotential layer. The electric field lines will be normal to the surface. The electric field is disturbed at points $Y_1$and Y_2 as it is seen from figures 4.3.2 and 4.3.3. The electric field at large distance from the surface remains unaffected by the presence of flying particle.

4.3.1 Electric Field Changes With Variation in Flying Particle Diameter

Figure 4.3.4 shows the effect of variation in diameter of flying particle on electric field distribution.The results are obtained with x_p= 2 p.u. i.e. the particle located at midway and h_p= 1mm i.e. particle elevated from the spacer surface by 1mm.

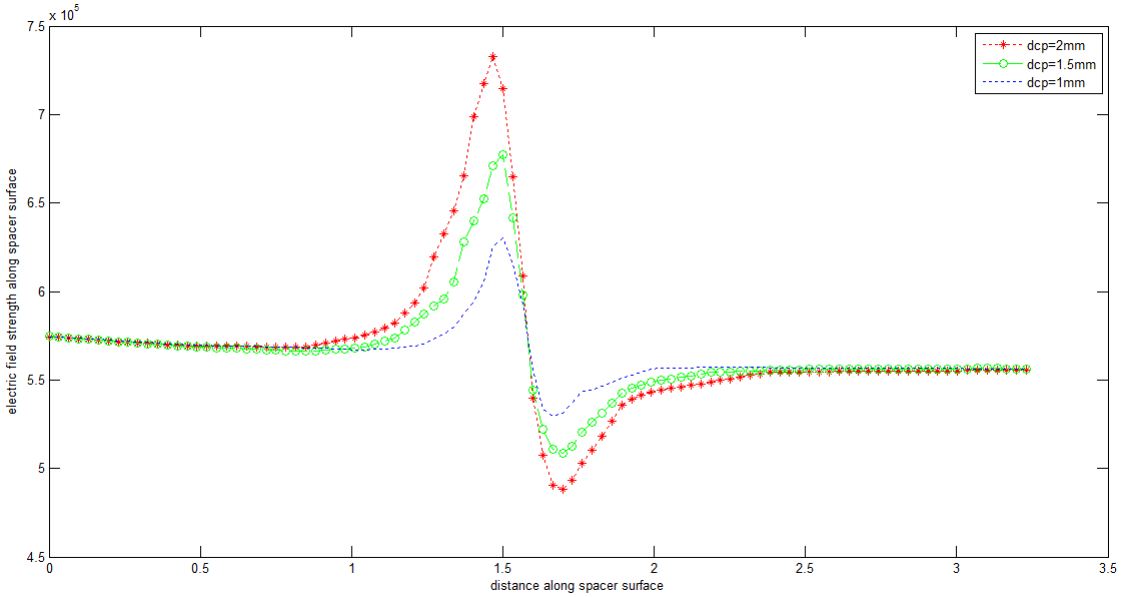

Figure 4.3.4: Electric Field with d_{cp}=1mm

It is observed that Defect Field Factor (DFF) decreases as the diameter of particle decreases.

Table 4.3: DFF variation with Flying Particle Diameter Variation

Diameter of Particle	Defect Field Factor (DFF)
2mm	1.36
1.5mm	1.18
1mm	1.12

4.3.2 Electric Field Changes With Variation in Particle Radial Location

The diameter of the particle is kept fixed at d_{cp}= 1mm and elevation at h_p= 1mm and radial positions are varied as 1.1pu, 1.5pu, 2pu, 2.5pu, 2.9pu. The electric field along the spacer surface for the respective cases is shown.

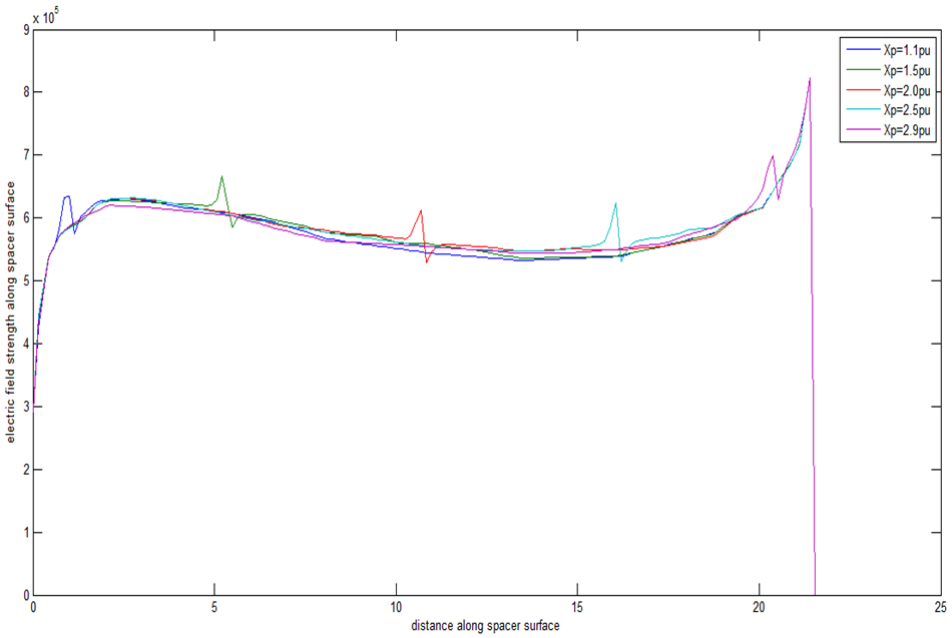

Figure 4.3.5: Electric Field with d_{cp}=1mm

DFF = 1.12 and is almost independent of location of flying particle.

4.3.3 Electric Field Changes With Variation in Particle Elevation

The particle radial location is kept fixed at x_p= 2 p.u. and diameter is kept constant at d_{cp}= 1 mm and particle vertical elevation from the spacer surface i.e. h_p is changed as 4 p.u. , 3 p.u. , 2 p.u. .The corroesponding changes in electric field distribution along the spacer surface are shown below.

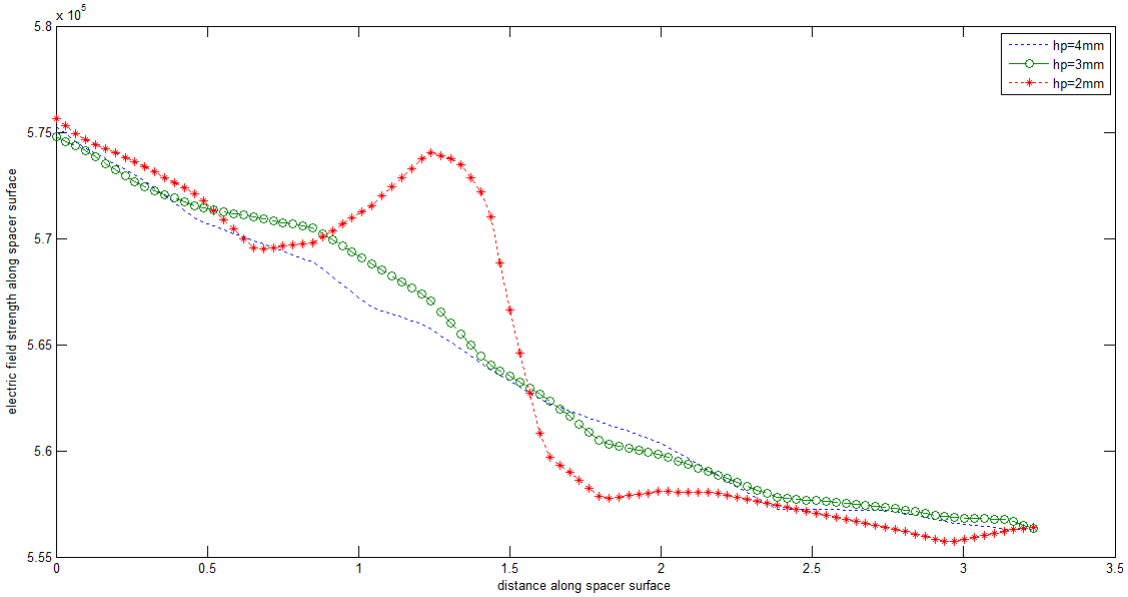

Figure 4.3.6: Electric Field with h_p= 2 mm.

It is observed that Defect Field Factor (DFF) decreases as the particle moves away from the spacer surface.

4.4 Adhered Particles

The adhered particles are attached to the surface of the spacer. So, they are modeled similar to the flying particles but the vertical elevation from the spacer surface i.e. h_p is taken to be zero.

4.4.1 Electric Field Changes With Variation in Adhered Particle Diameter

The effect of variation in diameter of adhered particle on electric field distribution is shown in figure 4.4.1 .The results are obtained with x_p= 2 p.u. i.e. the particle located at midway

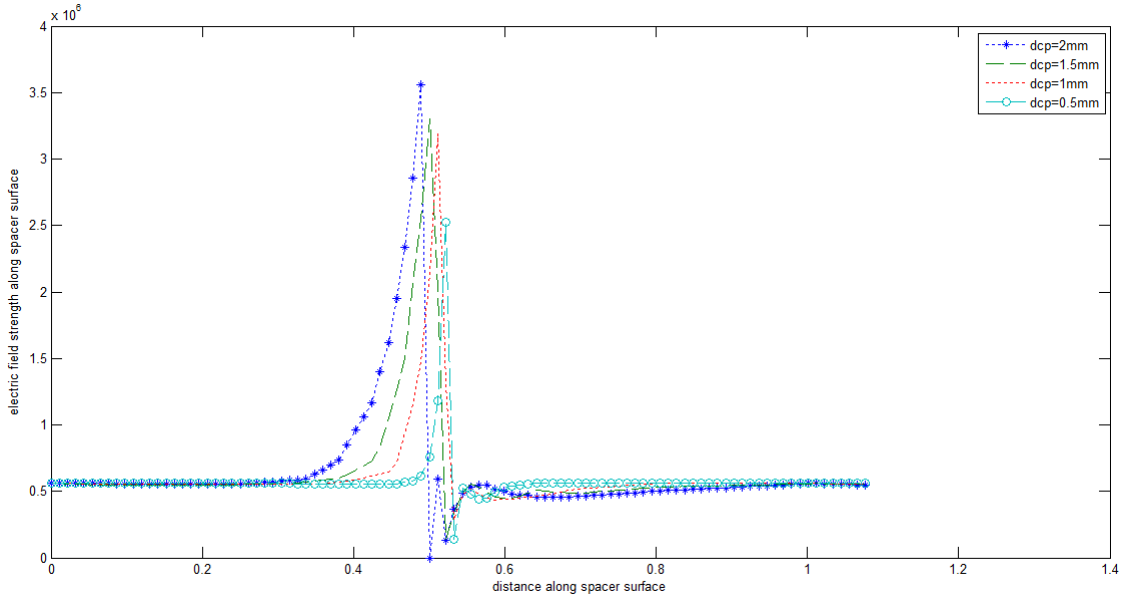

Figure 4.4.1: Electric Field Variation With Particle Diameter Variation

It is observed that Defect Field Factor (DFF) decreases as the diameter of particle decreases.

Table 4.4: DFF variation with Adhered Particle Diameter Variation

Diameter of Particle	Defect Field Factor (DFF)
2 mm	7
1.5 mm	6.5
1 mm	6.4
0.5 mm	5

4.5 Summary

Table 4.5: DFF variation with type of defect

Type of Defect	Maximum DFF
Protrusion	1.83
Depression	2.2
Flying Particle	1.36
Adhered Particle	7

From table 4.5, it is evident that adhered particles cause the highest amount of electric field distortion near the spacer surface.

Chapter 5

Conclusion And Future Work

5.1 Conclusion

5.1.1 Electromagnetic and Thermal Analysis

It is essential, from design point of view, to estimate the temperature distribution in the cross section of GIS when a particular value of steady state current flows through it. To study the same, GIS bus bar arrangement was considered. An AC current of same value (5000A) was allowed to flow through the conductor and the losses taking place in the main conductor and in the enclosure (due to induced eddy currents) were calculated using Maxwell Ansoft software. These loss values were then used as inputs for thermal analysis and the temperatures distribution across the cross section of GIS bus bar was calculated using Finite Element Method.

The loss in phase conductor is directly proportional to $\sqrt{\rho \, . \, \mu}$, where ρ is the resistivity of the metal (Ω . m) and μ is its magnetic permeability (H / m). Aluminium 6063 has the lowest value of $\sqrt{\rho \, . \, \mu}$. So, it is the most suitable metal for making the phase conductor. The loss in the enclosure is directly proportional to ρ, where ρ is the resistivity of the metal (Ω . m). Aluminium 6063 has the lowest value of ρ. So, it is best fit for making enclosure too.

Specifically for single phase bus bar arrangement, metal used for making the enclosure affects the temperature distribution across bus bar cross-section greatly. While, specifically for three phase bus bar arrangement, metal used for making the enclosure doesn't affect the temperature distribution across bus bar cross-section much. It mainly depends upon the value of current flowing through the phase conductors.

5.1.2 Electrostatic Analysis

For all types of spacer defects considered, the electric field gets more and more intensified at the defect location, as the diameter of the defect and the proxomity of the defect to the spacer surface increases. The highest value of DFF (Defect Field Factor) observed is 7 for a particle of diameter 2 mm adhered to the spacer surface. As the diameters of Protrusions and Depressions become less than 0.5 mm, the DFF (Defect Field Factor) observed is negligible. As the flying particles get away from the spacer surface, the DFF observed due to them is negligible typically when elevation becomes four times the diameter of the particle.

5.2 Future Work

5.2.1 Electromagnetic and Thermal Analysis

The value of resistivity of any material , ρ, depends upon temperature according to $\rho_T = \rho_o[\ 1 + \alpha.(\ T - T_o\ )]$. So, the value of resistivity will change with temperature and so will the resistance of the material and the losses produced in it. This coupling effect can be considered and more accurate values of electrical loss and consequently, of the temperature, be found.

5.2.2 Electrostatic Analysis

In this work, defects have been assumed to be axisymmetric type and 2D studies have been done. The same defects can be considered in 3D and more accurate graphs of electrical field distortion can be found.

References

[1] Siemens Energy Sector • Power Engineering Guide.

[2] Gas Insulated Substations by M S Naidu

[3] X. Wu, H. Li, Y. Peng, Z. Xie and X. Jin, "Temperature Distribution Analysis of Single-Phase GIS Bus," Power and Energy Engineering Conference (APPEEC), 2011 Asia-Pacific, Wuhan, 2011, pp. 1-4.

[4] H. K. Kim, Y. H. Oh and S. H. Lee, "Prediction of temperature rise in gas insulated busbar using multi-physics analysis," 2009 Transmission & Distribution Conference & Exposition: Asia and Pacific, Seoul, 2009, pp. 1-4.

[5] Joong-Kyoung Kim, Ji-Yeon Lee, Sang-Bong Wee and Sung-Chin Hahn, "A novel coupled magneto-thermal-flow analysis for temperature rise prediction of power apparatus," Electrical Machines and Systems, 2008. ICEMS 2008. International Conference on, Wuhan, 2008, pp. 585-588.

[6] Joong Kyoung Kim, Sung Chin Hahn, Kyong Yop Park, Hong Kyu Kim and Yeon Ho Oh, "Temperature rise prediction of EHV GIS bus bar by coupled magnetothermal finite element method," in IEEE Transactions on Magnetics, vol. 41, no. 5, pp. 1636-1639, May 2005.

[7] I K, Kim, et aL "Temperature rise prediction of EHV GIS bus bar by coupled magneto-thermal finite element method, " IEEE Trans" Magn" Vol 41, No, S, pp, 1636-1639, May 2005

[8] S. L. HO, "Analyses of Three-Dimensional Eddy Current Field and Thermal Problems in an Isolated Phase Bus, " IEEE Trans. Magn., vol. 39, no. 3, pp. 1515-1518, May 2003.

[9] S. L. HO, "Calculations of Eddy Current, Fluid, and Thermal Fields in an Air Insulated Bus Duct System, " IEEE Trans. Magn., vol. 43, no. 4, pp. 1433-1436, April 2007.

[10] H. K. Kim, et al., "Efficient technique for 3-D finite element analysis of skin effect in current-carrying conductors," IEEE Trans., Magn., Vol.40, No.2, pp. 1326-1329, March 2004

[11] S. W. Kim et al., "Coupled finite-element-analytic technique for prediction of temperature rise in power apparatus," in IEEE Transactions on Magnetics, vol. 38, no. 2, pp. 921-924, Mar 2002.

[12] C. C. Hwang, "Analysis of electromagnetic and termal fields for a bus duct system, " Electr. Power Syst. Res., vol. 45, no. 1, pp. 39-45, 1998.

[13] D. Labridis and V. Hatziathanassiou, "Finite element computation of field, forces and inductances in underground SF6 insulated cable using a coupled magnetothermal formulation", IEEE Trans. Magn., vol. 30, no. 4, pp. 1407-1415, 1994.

[14] I.A. Metwally, Reduction of electric-field intensification inside GIS by controlling spacer material and design, *Journal of Electrostatics* 70(2012) 217-224.

[15] Radwan, R.M., Abou-Elyazied and A.M., "Effect of Spacer's Defects and Conducting Particles on the Electric Field Distribution along Their Surfaces in GIS," in *Dielectrics and Electrical Insulation*, IEEE Transactions on , vol.14, no.6, pp.1484-1491, December 2007.

[16] I.A. Metwally, Status review on partial discharge measurement techniques in gas-insulated switchgears/lines, *Journal of Electric Power Systems Research* 69 (1) (2004) 25- 36.

[17] I.A. Metwally, Theoretical analysis of particle-initiated corona activities in hybrid gas-insulated transmission lines, *Journal of Electric Power Systems Research* 66 (2) (2003) 123-131.

[18] I.A. Metwally, A.A. A-Rahim, Dynamics of spherical metallic particles in electrostatic separators/sizers, *Journal of Electrostatics* 51 & 52 (2001) 252-258.

[19] B. Mazurek, J. D. Cross, and R. G. Van Heeswijk, "The effect of a metallic particle near a spacer on flashover phenomena in SF6", IEEE Trans. Dielectr. Electr. Insul. Vol. 28, pp. 219-229, 1993.

[20] Th. Baumann, B. Fruth, F. Stucki, and H. R. Zeller, "Field-enhancing defects in polymeric insulators causing dielectric aging", IEEE Trans. Dielectr. Electr. Insul. Vol. 24, pp. 1071-1078, 1989.

[21] A.K. Chakrabarti, R.G.V. Heeswijk, and K.D. Srivastava, Spacer involvement in conducting-particle-initiated breakdown in compressed gas insulated systems, IEEE Transactions on Electrical Insulation 22 (4) (1987) 431-438.

[22] IEEE Guide for Switchgear - Unit Substation - Requirements," in IEEE Std C37.121-2012 (Revision of IEEE Std C37.121-1989) , vol.15, no.18, pp.1-42, Feb. 22 2013.